Soft Matter

Directional Clogging and Phase Separation for Disk Flow Through Periodic and Diluted Obstacle Arrays

Journal:	*Soft Matter*
Manuscript ID	SM-ART-09-2020-001714.R2
Article Type:	Paper
Date Submitted by the Author:	02-Dec-2020
Complete List of Authors:	Reichhardt, Charles; Los Almaos, Reichhardt, Cynthia; Los Alamos National Laboratory, Theoretical Division

Journal Name

ARTICLE TYPE

Cite this: DOI: 00.0000/xxxxxxxxxx

Directional Clogging and Phase Separation for Disk Flow Through Periodic and Diluted Obstacle Arrays

C. Reichhardt and C. J. O. Reichhardt

Received Date
Accepted Date

DOI: 00.0000/xxxxxxxxxx

We model collective disk flow though a square array of obstacles as the flow direction is changed relative to the symmetry directions of the array. At lower disk densities there is no clogging for any driving direction, but as the disk density increases, the average disk velocity decreases and develops a drive angle dependence. For certain driving angles, the flow is reduced or drops to zero when the system forms a heterogeneous clogged state consisting of high density clogged regions coexisting with empty regions. The clogged states are fragile and can be unclogged by changing the driving angle. For large obstacle sizes, we find a uniform clogged state that is distinct from the collective clogging regime. Within the clogged phases, depinning transitions can occur as a function of increasing driving force, with intermittent motion appearing just above the depinning threshold. The clogging is robust against the random removal or dilution of the obstacle sites, and the disks are able to form system-spanning clogged clusters even under increasing dilution. If the dilution becomes too large, however, the clogging behavior is lost.

There are a variety of systems that can be described as a loose assembly of particles which exhibit jamming behaviors. At lower densities, flow occurs easily in such systems, but at high densities the system can act like a solid in which all flow ceases[1–6]. Jamming has been extensively studied as a function of density[1,3], shear[6], particle shape[5,7–9], and friction effects[10,11]. Many of these studies involved no quenched disorder so that the system can be described as containing only particle-particle interactions. It is also possible for the particle motion to be stopped by some form of external constraints, such as flow through bottlenecks or funnels[12–17], motion through a mesh[18–22], flow over a disordered substrate[23–25], or flow in porous media[26–32]. The particle flow stops when the combination of the particle density and the obstacle density is high enough. Open questions include identifying when the cessation of flow in specific systems with quenched disorder can be described as jamming, clogging, or depinning, as well as how to distinguish between these phenomena.

There are several limiting cases for jamming and clogging behavior. For example, frictionless disks have a well defined jamming density ϕ_J in the absence of obstacles. If a small number of obstacles are added, in the high density limit the system can still be described as reaching a jamming point at a slightly lower density $\phi < \phi_J$ due to the diverging length scale l_J that emerges as the jamming density in the clean system is approached[1–4]. Jamming, which is associated with a uniform particle density throughout the system, occurs once the average distance between obstacles $l_{\rm obs}$ becomes smaller than the jamming length scale $l_{\rm obs} < l_J$. This has been studied in several systems in the limit of high particle density and low obstacle density.

Another limit is the clogging of a single particle, which can arise for flow along the x direction through a square array of obstacles when the obstacle radius becomes large enough that the particle cannot fit in the space between adjacent obstacles. Between the jamming and single particle clogging limits, a variety of other types of collective clogging behaviors are possible in which groups of particles come together to create a locally stuck region.

Several studies addressing the effects of a small number of obstacles or weak quenched disorder on the jamming transition show that the jamming density decreases as obstacles are added[33–35], while other studies have focused on a crossover from jamming to clogging behavior for particles moving through obstacle arrays[36–39]. Péter *et al.*[37] considered an assembly of monodisperse particles moving over a random obstacle array. For a small number of obstacles, they found jamming behavior in which the particle density is uniform in the motionless state. Once the obstacle density exceeds a certain threshold, there is a crossover from jamming to clogging behavior, with the clogging persisting down to very low particle densities. The clogged state is highly heterogeneous and contains local patches in which the particle density is close to the jamming density along with other patches in which there are few or no particles. Additionally, the system requires time in which to organize organize into a particular clogged configuration, whereas the jammed states form very rapidly. Nguyen *et al.*[36] studied an assembly of bidisperse grains moving through

Theoretical Division and Center for Nonlinear Studies, Los Alamos National Laboratory, Los Alamos, New Mexico 87545, USA. Tel: +1 505 665 1134; E-mail: cjrx@lanl.gov

a two-dimensional periodic obstacle array and also found a transition to a clogged state characterized by the formation of a high density phase coexisting with a low density phase. In this case, the susceptibility to the formation of a clogged state depended on the direction of the flow relative to the substrate symmetry directions. For example, when the obstacles are small, the system does not jam when driven along the x-direction, but for driving along $30°$, the system can reach a clogged or partially jammed state. In experimental work, Stoop *et al.*[38,39] studied the motion of colloidal disks through a random array of obstacles. They found that the flow decreases over time due to the gradual formation of clogged regions.

In this work we examine monodisperse disks moving through a periodic array of obstacles under an external drive that varies in direction from $0°$ to $90°$ from the x axis. For low disk densities, the disks flow for every direction of applied drive; however, the net velocity drops at incommensurate angles and reaches a maximum for drives along the easy flow directions of $0°$, $45°$ and $90°$. When the disk density is increased, we find that although flow still occurs for driving near $0°$ and $90°$, the system begins to clog at the intermediate angles by forming a phase separated state containing regions of high and low disk density. The clogged system is fragile in nature[40], and we find a partial hysteresis effect in which the flow can resume if the driving angle is changed after the clogged state forms. We map the locations of the clogged states as a function of obstacle size, and show that there is a critical obstacle size above which even single disks become clogged for driving along the incommensurate directions. We find that a clogged state can undergo a depinning transition to a flowing state if the driving force is increased. Just above the depinning transition, the flow is intermittent and there is a coexistence of clogged states and moving states; however, the moving disks do not exchange neighbors, indicating that the depinning transition is elastic[41]. These results show that clogging is associated with changes in the packing that result from modifying either the mobile disk density or the obstacle density, while depinning is associated with changing the driving force for a system that is already in a heterogeneous or uniform clogged state.

We find that the clogged states are fairly robust to dilution of the obstacle lattice as long as large scale system-spanning dense clusters can still occur; however, when the dilution becomes extensive, the system flows instead of clogging.

Experimental systems in which our results could be tested include particle flow through periodic obstacle arrays[42–47] or optical trap arrays[48–52]. Most previous works in such systems were performed in the low density regime where particle-particle interactions are weak. Clogging behavior is expected to occur for high particle densities or in regimes where the diameter of the obstacles is large.

Simulation

We model a two dimensional $L \times L$ system containing a square array of obstacles with lattice spacing a and obstacle radius $r_{\rm obs}$. We fix $L = 36$ and $a = 4.0$. Within the system we place N_d mobile disks with dynamics given by the following overdamped equation of motion:

$$\alpha_d \mathbf{v}_i = \mathbf{F}_i^{dd} + \mathbf{F}_i^{obs} + \mathbf{F}_i^{D}. \quad (1)$$

The velocity of disk i is $\mathbf{v}_i = d\mathbf{r}_i/dt$, the disk position is $\mathbf{r}_i$, and the damping constant α_d is set to $\alpha_d = 1.0$. The disk-disk interaction force $\mathbf{F}_i^{dd}$ arises from a harmonic repulsive potential with radius r_d, which we fix to $r_d = 0.5$. We set the strength of the harmonic repulsion to $k = 30$, which is strong enough that there is only weak overlap of the disks for the driving forces we consider in most of the paper; however, when we study depinning, the finite harmonic force allows small distortions of the disks to occur. The disk-obstacle force $\mathbf{F}^{obs}$ is also modeled with a repulsive harmonic potential with the same strength k. The system density is defined as the total area covered by the obstacles and mobile disks, $\phi = N_{\rm obs}\pi r_{\rm obs}^2/L^2 + N_d \pi r_d^2/L^2$, where $N_{\rm obs}$ is the number of obstacles. The external drive $\mathbf{F}_D = F_D[\cos(\theta)\hat{\mathbf{x}} + \sin(\theta)\hat{\mathbf{y}}]$ is initially applied along the x-direction and gradually rotates from $\theta = 0°$ to $\theta = 90°$ or higher. We measure the average velocity of all of the mobile disks in the x-direction, $\langle V_x \rangle = N_d^{-1}\langle \sum_{i=1}^{N_d} \mathbf{v}_i \cdot \hat{\mathbf{x}} \rangle$, where the average is taken over a time of 25000 simulation time steps, and in the y-direction, $\langle V_y \rangle = N_d^{-1}\langle \sum_{i=1}^{N_d} \mathbf{v}_i \cdot \hat{\mathbf{y}} \rangle$, as well as the net velocity $\langle V \rangle = \sqrt{\langle V_x \rangle^2 + \langle V_y \rangle^2}$. We also plot the mobility $M = \langle V \rangle/(\alpha_d|F_D|)$, which has the value $M = 1$ for a disk that is flowing freely without striking any other disks or obstacles. Similarly, we measure $M_x = \langle V_x \rangle/(\alpha_d|F_D|)$ and $M_y = \langle V_y \rangle/(\alpha_d|F_D|)$. For low drives, the system behavior is close to the hard disk limit, while for higher drives the behavior is closer to what one would find for bubbles or emulsions. Our parameters are dimensionless, but a reasonable comparison to experiment can be made for the system used by Stoop and Tierno[38], where the particles are of radius 1.3 μm, the obstacles are of radius 2 μm, the lattice periodicity is 4 to 5 μm, and the velocities are in the range of 0 to 10 μm/s.

We find that the dynamics can depend on the rate at which the drive direction is changed, so we consider the limit where the direction is changed slowly enough that such effects are absent, which for our parameters is $\delta\theta = 0.000125$ applied every 25000 simulation time steps. In previous work we examined lower disk densities where the system is in the flowing state and exhibits a series of directional locking effects where the disks preferentially flow along specific symmetry directions of the obstacle lattice[53]. Here we focus on large obstacle sizes and/or large disk densities where clogging effects appear.

Directional Clogging and Memory Effect

We first consider a system with $r_{\rm obs} = 1.485$ at $F_D = 0.0025$. In Fig. 1(a) we plot M versus θ at $\phi = 0.632$ where there are $N_{\rm obs} = 81$ obstacles and $N_d = 330$ mobile disks. If the disks were flowing freely without contacting the obstacles or other disks, we would obtain $M = 1.0$. Figure 1(a) shows that M is finite for all driving angles, indicating that the system is never in a clogged state; however, local maxima in M appear at $\theta = 0°$, $45°$, and $90°$. At these symmetry directions of the substrate array, the disks can minimize the number of collisions that occur with the obstacles, as studied previously[53]. Local maxima of mobility are expected to be centered at angles $\theta = \tan^{-1}(p/q)$, where p and q are integers, and as the obstacle radius or the number of mobile disks

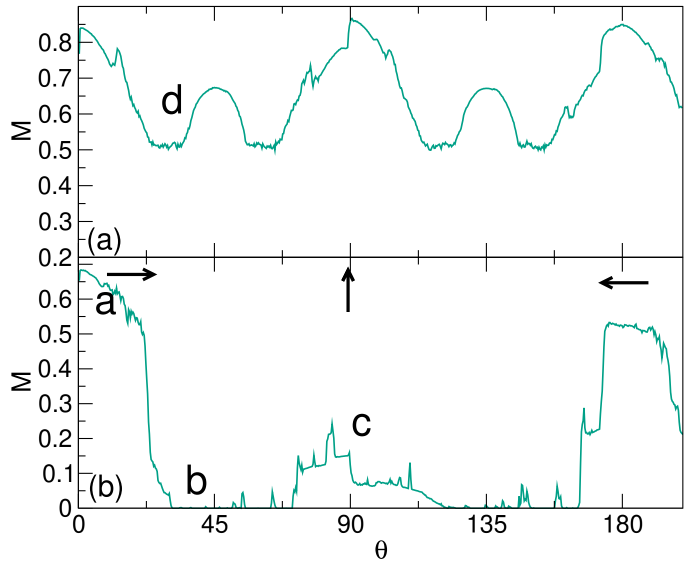

Fig. 1 The value of the mobility M per particle vs driving direction θ for mobile disks moving through a square obstacle array with $r_{\rm obs} = 1.485$ at $F_D = 0.0025$. (a) At a total system density of $\phi = 0.632$, the disks are always flowing but M has local maxima at $\theta = 0^\circ$, 45° and 90°. (b) At $\phi = 0.68$, there are extended regions where the system is in a clogged state. The labels (a,b,c,d) indicate the values of θ at which the images in Fig. 2 were obtained. The arrows indicate the direction of the driving force, which is in the positive x direction when $\theta = 0^\circ$, the positive y direction for $\theta = 90^\circ$, and the negative x direction when $\theta = 180^\circ$.

decreases, more of these mobility maxima appear in the M versus θ curve [53]. In Fig. 1(a), the maximum value of $M = 0.84$ occurs for $\theta = 90^\circ$, where all the disks are flowing but the collisions cause a reduction in the velocity compared to an obstacle-free system. The minimum value of $M = 0.5$ falls near $\theta = 30^\circ$ where there are regions of the sample in which some disks are completely stuck while in other regions of the sample the disks continue to move.

In Fig. 1(b), we plot M versus θ for the same system with a larger number $N_d = 409$ of mobile disks, giving $\phi = 0.68$. There are now extended regions of $M = 0.0$ in which the system is in a clogged state, such as for $30^\circ < \theta < 70^\circ$ and $120^\circ < \theta < 167^\circ$. In other intervals of θ, the disks are still able to flow, such as for driving along the 0° and 90° symmetry directions of the obstacle array. The maximum value of $M = 0.68$ appears at $\theta = 0^\circ$. There is then a drop in mobility with a value of $M = 0.15$ at $\theta = 90^\circ$, followed by an increase of mobility back to $M \approx 0.53$ for $\theta = 180^\circ$. The mobility has a similar value for driving in the positive or negative x direction but is considerably smaller for driving in the y direction. This hysteresis or memory of the initial driving direction results from the fragility of the clogged states. When the disks first form a clogged phase at $\theta = 30^\circ$, they become locked to a configuration that blocks flow for driving along or close to that particular value of θ. When θ increases to 90°, a portion of the configuration remains clogged so the flow is reduced compared to its original $\theta = 0^\circ$ value. As θ increases to $\theta = 180^\circ$, along the negative x direction, the drive exerts reversed forces on the configurations that formed to block the $\theta = 30^\circ$ flow, destroying these configurations and unclogging the system. When we continue to cycle the value of θ, we always find greater flow along the $\pm x$ directions than along the $\pm y$ directions. If we instead initially drive the system with $\theta = 90^\circ$ so that the flow is along the y direction, we find the opposite effect in which the flow is always higher along the $\pm y$ directions than along the $\pm x$ directions. This indicates that the flow retains a memory of the initial driving direction. For $\phi = 0.632$ in Fig. 1(a), M exhibits little or no memory effect since no clogging occurs, so the values of M at $\theta = 0^\circ$ and $\theta = 90^\circ$ are nearly identical.

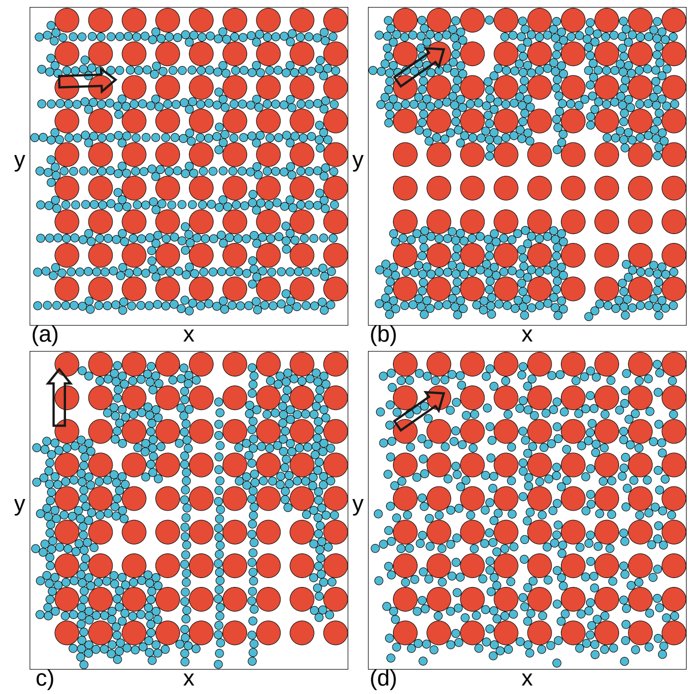

Fig. 2 The obstacle locations (red circles) and mobile disks (blue circles) for the system in Fig. 1(b) with $r_{\rm obs} = 1.485$, $F_D = 0.0025$, and $\phi = 0.68$ at (a) $\theta = 2^\circ$ where the disks are flowing along the x direction, (b) $\theta = 35^\circ$ where the system is in a clogged state, and (c) $\theta = 90^\circ$ where there is a combination of clogged and flowing disks. (d) The same for the system in Fig. 1(a) with $\phi = 0.632$ at $\theta = 35^\circ$ where a clogged state does not occur. The arrows indicate the direction of the driving force.

In Fig. 2(a) we show a snapshot of the disk and obstacle locations for the system in Fig. 1(b) at $\theta = 2^\circ$ where the disks are flowing along the x direction. Figure 2(b) illustrates the clogged configuration at $\theta = 35^\circ$ where all the disks are immobile and have formed high density regions coexisting with regions that contain no mobile disks. In Fig. 2(c) at $\theta = 90^\circ$, clogged configurations coexist with moving disks which are aligned with the y direction and flowing in the driving direction near the center of the sample. Figure 2(d) shows the obstacle and disk configurations at $\theta = 35^\circ$ for the system in Fig. 1(a) where no clogged state appears and the disk density remains uniform. If we consider different initial random positions for the disks, we find the same general features; however, the smaller spike features in Fig. 1(b) shift to different locations since these are produced by the detailed positioning of the disks.

As ϕ decreases, the clogging memory effect diminishes, as shown in the plot of M versus θ in Fig. 3(a) for a sample with $\phi = 0.656$. There are two clogged windows, but in the moving

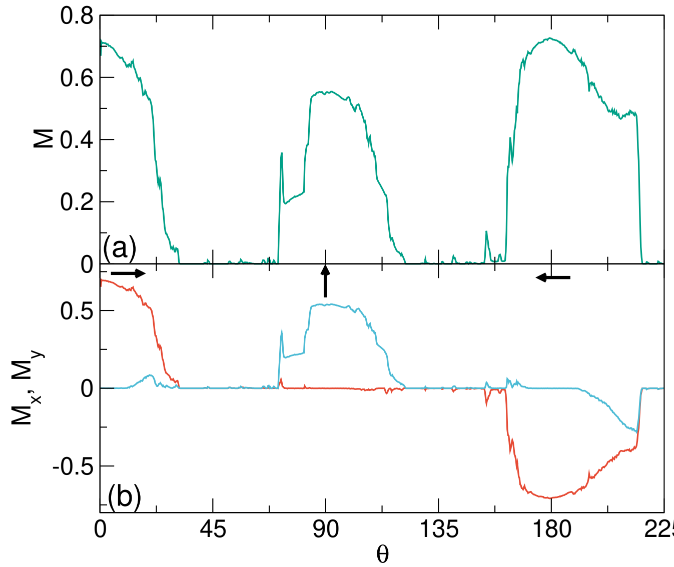

Fig. 3 (a) M vs θ for the same system in Fig. 1 with $r_{\rm obs} = 1.485$ and $F_D = 0.0025$ but at a lower $\phi = 0.656$ showing two clogged regimes and a reduction of the memory, as indicated by the fact that the mobility is nearly the same for $\theta = 0°$ and $\theta = 90°$. (b) The individual mobility components M_x (red) and M_y (blue) vs θ showing that the flow in the non-clogged regions occurs preferentially along the x or y directions. The arrows indicate the direction of the driving forces at $\theta = 0°$, $90°$ and $180°$.

regimes, the velocity is nearly equal in magnitude for both $\theta = 0°$ and $\theta = 90°$. In Fig. 3(b) we plot the corresponding velocity components M_x and M_y versus θ. When $\theta < 30°$, the flow is predominantly along the x direction, but there is a small amount of motion in the y direction produced by the disk rearrangements that occur as the system enters the clogged state. Both velocity components are zero in the clogged regime. For $70° < \theta < 120°$, the flow is almost exclusively along the y direction since the clogged state formed for driving along the x direction, causing motion along x to be suppressed. The x direction mobility becomes negative near $\theta = 180°$ since the driving force is aligned in the negative x direction, as indicated by the arrows.

The memory effect continues to diminish with decreasing ϕ as shown in Fig. 4 where we plot $\langle V \rangle$ versus ϕ at $\theta = 0°$ and $\theta = 90°$. When the system retains a memory of the driving direction, the net velocity for these two driving directions is different. When $\phi < 0.63$, clogging becomes impossible and the memory effect disappears. The reduced velocity magnitude found at 90° is approximately repeated when the drive reaches 270°, but the velocity is generally slightly smaller after each driving cycle. We have tested this up to four driving cycles. It may be possible that if N driving cycles were applied, the system would settle into a reversible state similar to that found for the memory effects in ac driven systems such as sheared dilute colloids and amorphous solids; however, further exploration of this effect is deferred to a later work.

The ability of the system to clog at a fixed mobile disk radius is determined by the driving direction θ, the total density ϕ, and the obstacle radius $r_{\rm obs}$. Additionally, as we show below, a clogged system can be unclogged by increasing the magnitude of the force to produce a depinning transition. The directional dependence of the clogging arises from the changes in the effective distance $a_{\rm eff}$

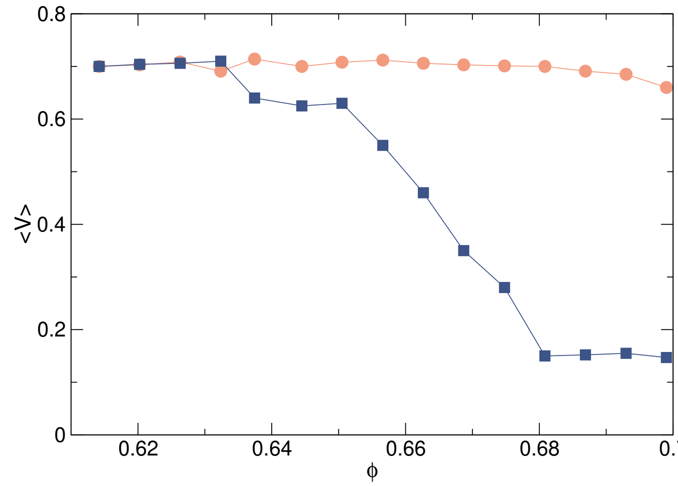

Fig. 4 $\langle V \rangle$ versus density ϕ for the system in Fig. 1 with $r_{\rm obs} = 1.485$ and $F_D = 0.0025$ at $\theta = 0°$ (orange circles) and $\theta = 90°$ (blue squares). A memory effect in which the velocity at the two values of θ is different appears when $\phi > 0.63$.

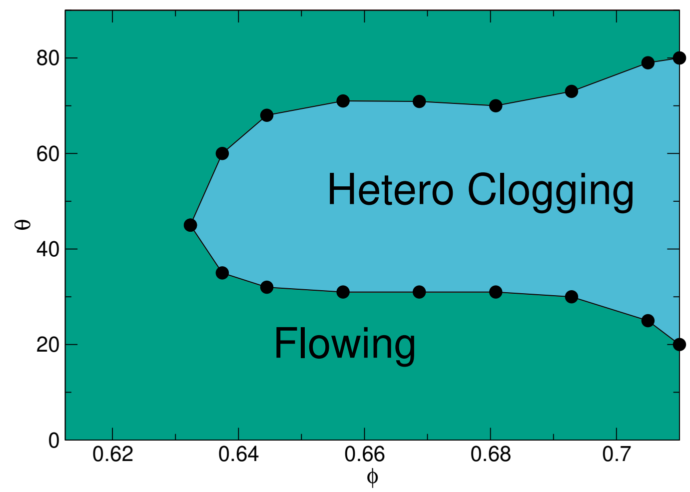

Fig. 5 Dynamical phase diagram as a function of θ versus ϕ for the system in Fig. 1 with $r_{\rm obs} = 1.485$ and $F_D = 0.0025$ showing the heterogeneous clogging regime (green) and the flowing regime (blue).

between obstacles along the path of the mobile disks. For $\theta = 0°$ and $\theta = 90°$, $a_{\rm eff}$ reaches its maximum value of $a_{\rm eff} = a$, while at incommensurate angles, $a_{\rm eff}$ is reduced, permitting more frequent collisions between the mobile disks and the obstacles. In Fig. 5 we plot a dynamical phase diagram as a function of θ versus ϕ for the system in Fig. 1 highlighting where the heterogeneous clogged state appears. For $\phi < 0.63$, the system never clogs, while as ϕ increases above $\phi = 0.63$, the width of the clogging phase increases. For $\phi > 0.71$ our initialization procedure cannot pack any more disks into the system; however, we expect that for high disk densities the width of the clogged state would continue to grow until the system becomes jammed for all directions of motion which, in the absence of obstacles, would occur close to $\phi = 0.9$. The formation of a jammed rather than a clogged state would also be associated with the loss of the memory effect since the velocity would be zero for every direction of drive. The nature of the change from clogging to jamming behavior is beyond the scope of the present study. The fragility that we observe in the clogged phase is consistent with the ideas of fragility proposed for certain types of soft matter systems under constraints, where special configurations or force chains must form to block the flow in certain directions[40].

Clogging for Varied Obstacle Size

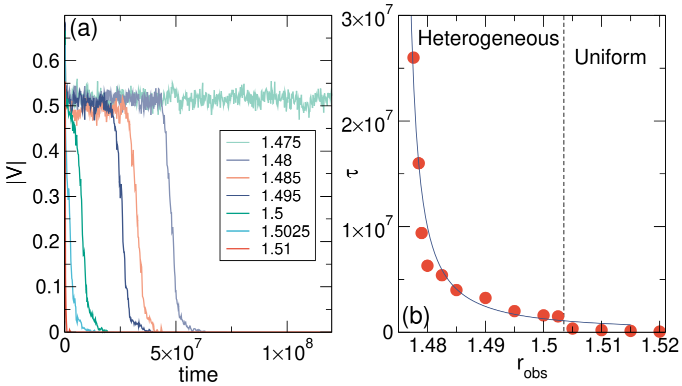

Fig. 6 (a) Instantaneous velocity V versus time in simulation time steps for the system in Fig. 1 with $F_D = 0.0025$ and fixed driving angle $\theta = 31^\circ$ for obstacle radius $r_{\rm obs} = 1.51$ (dark orange), 1.5025 (light blue), 1.5 (dark green), 1.495 (dark blue), 1.485 (light orange), 1.48 (light purple), and 1.475 (light green). (b) The time τ for the system to reach a clogged state vs $r_{\rm obs}$. The solid line is a fit to $\tau \propto (r_{\rm obs} - r_c)^{-1.25}$. The dashed line separates the heterogeneous clogging state from the uniform clogged state.

In Fig. 6(a) we plot the instantaneous disk velocity V versus time in simulation time steps for the system in Fig. 1(b) at a fixed drive direction of $\theta = 31^\circ$ with varied obstacle sizes of $r_{\rm obs} = 1.51$, 1.5025, 1.5, 1.495, 1.485, 1.48, and 1.475. The time needed for the system to reach a zero velocity clogged state increases with decreasing $r_{\rm obs}$. We find two distinct clogging regimes as a function of $r_{\rm obs}$ for this obstacle density. When $r_{\rm obs} > 1.502$, the spacing between adjacent obstacles is so small that even a single disk can become trapped when attempting to move between the obstacles. The obstacle lattice constant is $a = 4.0$ and the mobile disks have radius $r_d = 0.5$, so there is only exactly enough room for the mobile disk to pass between the obstacles without touching them when $r_{\rm obs} = 1.5$. Since the disk-obstacle interaction is represented by a very stiff spring rather than a hard wall, disks can still slip between the obstacles even when $r_{\rm obs} > 1.5$. We define the obstacle radius at which the a particle cannot move through the lattice as r_σ, which is a function of the obstacle lattice constant and the radius of the mobile disk. In this example, $r_\sigma = 1.502$. For $r_{\rm obs} > r_\sigma$, the clogging occurs at the single disk level and is uniform in nature, while for $1.475 < r_{\rm obs} < r_\sigma$, multiple mobile disks must interact in order to form a clogged state, resulting in spatial heterogeneity. For $r_{\rm obs} < 1.475$, the system is in a flowing state. In the heterogeneous clogging regime, the initial flowing state persists for some time before a collision between mobile disks nucleates a high density clogged region that can spread across the sample, blocking the flow.

In Fig. 7 we illustrate some representative configurations for the system in Fig. 6. Figure 7(a) shows a uniformly clogged state

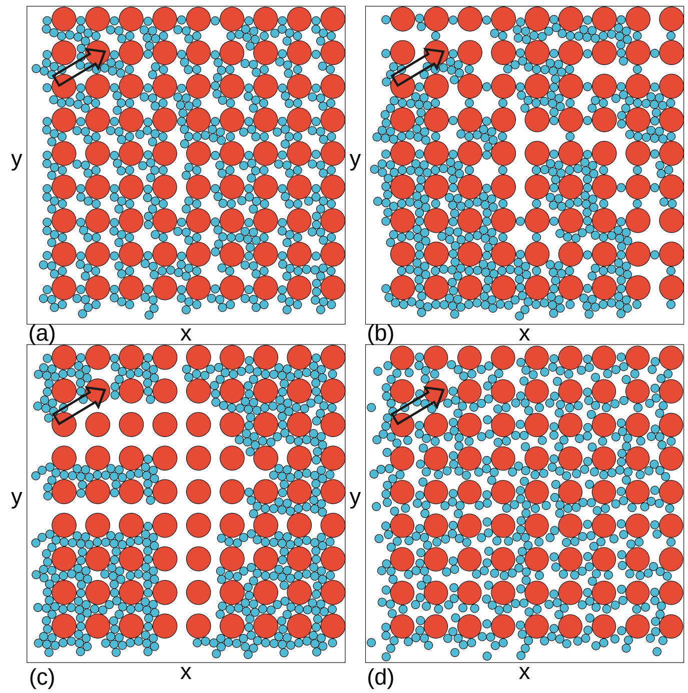

Fig. 7 The obstacle locations (red circles) and mobile disks (blue circles) for the system in Fig. 6 with $F_D = 0.0025$ and $\theta = 31^\circ$ where r_σ, the radius at which a single particle cannot move between two obstacles for this obstacle lattice constant, is $r_\sigma = 1.502$. (a) A uniform or homogeneous clogged state at $r_{\rm obs} = 1.51$. (b) A clogged state for $r_{\rm obs} = 1.5025$ at the crossover from uniform to heterogeneous clogging. (c) A heterogeneous clogged state at $r_{\rm obs} = 1.5$. (d) A flowing state at $r_{\rm obs} = 1.45$.

at $r_{\rm obs} = 1.51$, where the disks are all immobile but the density is uniform. At $r_{\rm obs} = 1.5025$ in Fig. 7(b), there is a transition to heterogeneous clogging. In Fig. 7(c) we show a heterogeneous clogged state at $r_{\rm obs} = 1.5$, while at $r_{\rm obs} = 1.45$ in Fig. 7(d), the disks are flowing.

We measure the time τ required for the system to reach a clogged state by fitting the curves in Fig. 6(a) to the form $V(t) \propto \exp -t/\tau + V_0$. In Fig. 6(b) we plot τ versus $r_{\rm obs}$, showing a divergence near a critical obstacle radius of $r_c = 1.4752$. The solid line is a fit to $\tau \propto (r_{\rm obs} - r_c)^\gamma$ with $\gamma = -1.25$. When $r_{\rm obs} > 1.5025$, τ drops to a small value since no plastic rearrangements are required for the system to reach a uniform clogged state. The dashed line indicates the transition from the heterogeneous to the uniform clogging behavior. The range of the power law fit is limited so the results should be regarded with some caution. The power law divergence in τ near r_c resembles the time divergence found at reversible to irreversible transitions in periodically sheared colloidal systems[54,55], amorphous solids[56], and superconducting vortices[57]. In previous numeral work on clogging in two-dimensional random obstacle arrays[37], a similar power law time divergence with an exponent of $\gamma = -1.29$ appeared when the system entered the clogged phase as the obstacle density was varied. These exponents are close to the value expected for an absorbing phase transition, where the clogged state can be viewed as the absorbed state since in this state all fluctuations are lost[58].

When the obstacles are in a periodic array, the nature of the clogged state depends on the driving direction. For $\theta = 0^\circ$ or

$\theta = 90^\circ$, there is only a uniform clogged state for $r_{obs} > 1.5025$ but there are no heterogeneous clogged states, so we find no power law divergence in the clogging time for these driving directions. At incommensurate angles, the system has a closer resemblance to a random obstacle array, making it possible for a heterogeneous clogged state to appear that is associated with a power law divergence in the time required for the clogged state to organize. In this work we focus only on monodisperse mobile disks, but if the mobile disk radii were bidisperse or multidisperse, the system could exhibit heterogeneous clogging for x and y-direction driving. In this case, the clogging transition would likely shift to lower values of ϕ and r_{obs}.

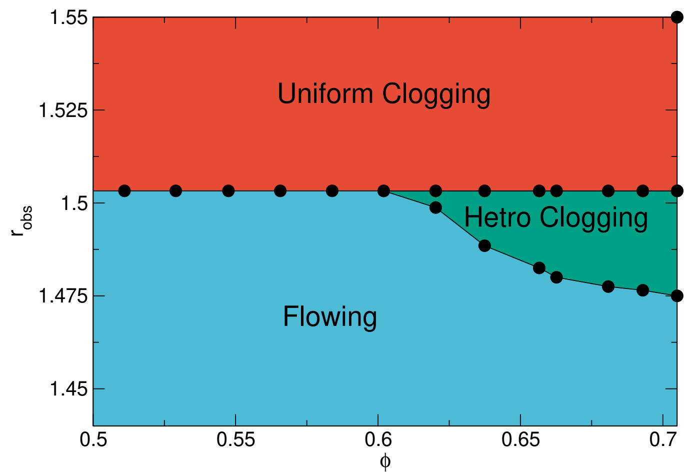

Fig. 8 Dynamical phase diagram as a function of r_{obs} vs ϕ for the system in Fig. 6 with $F_D = 0.0025$ and fixed driving angle $\theta = 31^\circ$ showing the heterogeneous clogging regime (green), flowing regime (blue), and uniform clogging regime (red).

In Fig. 8 we plot a dynamical phase diagram as a function of r_{obs} versus ϕ for the system in Figs. 6 and 7 where the drive is applied at $\theta = 31^\circ$. For $r_{obs} > 1.503$, the system forms a uniform clogged state that is independent of ϕ, and the clogged state forms immediately with no diverging time scale. When $\phi > 0.6$ and $1.475 < r_{obs} < 1.5032$, we find heterogeneous clogging with a power law time divergence for the formation of the clogged state. Similar phase diagrams can be constructed for other driving angles. For example, at $\theta = 0^\circ$ the heterogeneous clogged phase is absent for the same range of system parameters shown in Fig. 8.

In our studies we have not considered the effect of temperature or other perturbations such as activity[59,60]. Such perturbations are likely to wash out the clogged state due to its fragile nature; however, there could still be some remnant of nonlinear behavior or intermittent dynamics in regions where heterogeneous clogging would occur in the absence of the perturbations.

Depinning of the Clogged Phase

Since the disk-disk interactions in our system have a harmonic form, the clogged phase should exhibit a drive dependence or a critical driving force above which it should unclog or depin. This type of depinning or unclogging effect is applicable to systems such as bubbles, emulsions, soft colloids, or magnetic bubbles. On the other hand, in granular matter or other systems with hard core particle-particle interactions where the particles cannot deform easily, such depinning would likely occur only for much higher drives and would be difficult to access experimentally.

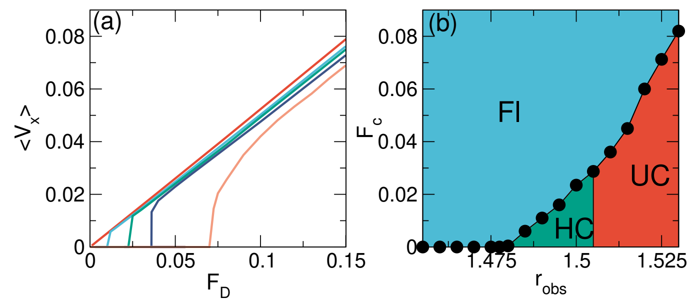

Fig. 9 (a) The average velocity $\langle V_x \rangle$ vs F_D for the system in Fig. 1 with a drive angle of $\theta = 33.8^\circ$ and a fixed number of disks and obstacles giving $\phi = 0.68$ at $r_{obs} = 1.475$ for varied obstacle size $r_{obs} = 1.525$ (orange), 1.51 (dark blue), 1.5 (green), 1.49 (light blue), and 1.475 (orange red). (b) The depinning threshold F_C vs r_{obs} for the system in (a). Colors indicate the flowing regime (blue), heterogeneous clogging regime (green), and uniform clogging regime (red).

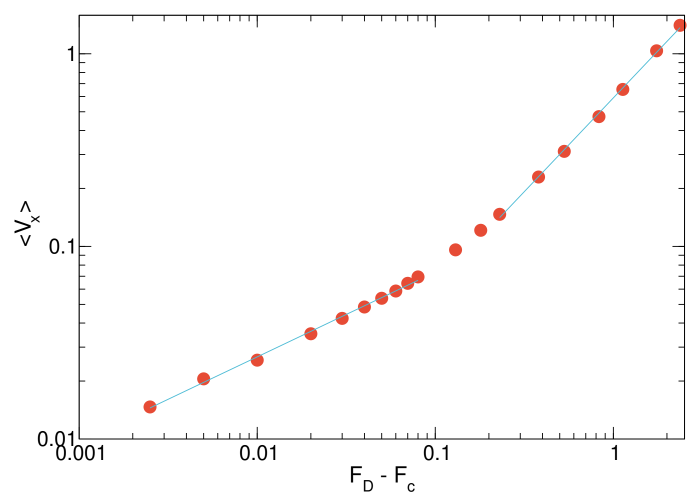

Fig. 10 The scaling of the velocity-force curve from Fig. 9(a) plotted as $\langle V_x \rangle$ vs $F_D - F_c$ in the uniform clogged phase at $r_{obs} = 1.525$, where $F_C = 0.07$. Here $\phi = 0.68$ and $\theta = 33.8^\circ$. The leftmost solid line is a power law fit with $\beta = 0.44$, while at higher drives, there is a crossover to a linear behavior with $\beta = 0.97$, as indicated by the rightmost solid line.

In the previous sections, we considered a drive force of $F_D = 0.0025$ which is well below the depinning threshold. We now sweep the value of F_D to explore the depinning behavior. In Fig. 9(a) we plot $\langle V_x \rangle$ versus F_D for the system in Fig. 1 at a fixed number of obstacles and a fixed mobile disk number corresponding to a density of $\phi = 0.675$ when $r_{obs} = 1.475$ at $r_{obs} = 1.525$, 1.51, 1.5, 1.49, and 1.475. In Fig. 9(b) we plot the depinning threshold F_c versus obstacle size. The depinning threshold becomes finite for $r_{obs} > 1.475$, and increases with increasing r_{obs}.

At $r_{obs} = 1.525$, the velocity-force curve has an upward concavity and can be fit to the form $V = (F_D - F_c)^\beta$ with $\beta = 0.44$, as shown in the left side of Fig. 10. In general, systems that exhibit elastic depinning have a depinning exponent of $\beta < 1.0$[41]. When the clogged state undergoes depinning, the disks maintain their same neighbors and there is no plastic flow. The resulting elastic depinning process arises because the obstacles are large enough that the moving disks do not have any space to pass one another, forcing the disks to flow in 1D channels without exchanging neighbors. At higher drives, the velocity crosses over to a linear form with $V \propto F_D$, as shown in the right side of Fig. 10 which illustrates a fit with $\beta = 0.97$. We generally find that depinning in the uniform clogging phase is elastic, and that the disk density remains uniform in both the pinned and flowing states. Depinning in the heterogeneous clogged phase is more consistent with a discontinuous jump, which could be indicative of a first order type of transition. Here the pinned state is phase separated but the flowing state has a uniform disk density. This result is consistent with work which shows that the depinning of two-dimensional phase separated systems has a first order character when either the pinned state is phase separated and the flowing state is uniform or the pinned state is uniform and the flowing state is phase separated[61,62].

Fluctuations

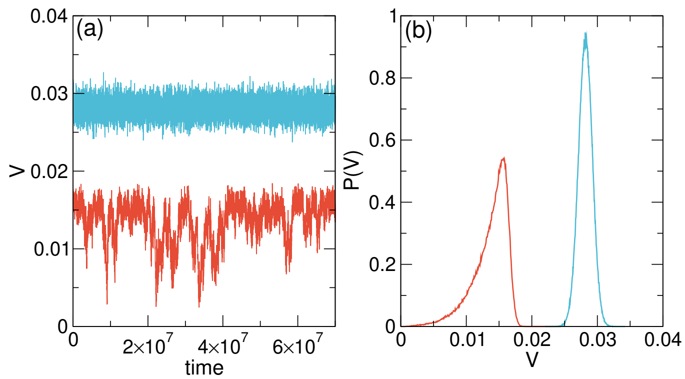

Fig. 11 (a) Instantaneous velocity V vs time in simulation time steps for the system in Fig. 9(a) with $\phi = 0.68$, $\theta = 33.8^\circ$, and $r_{\rm obs} = 1.51$ at $F_D/F_C = 1.0034$ (red) and $F_D/F_C = 1.67$ (blue). (b) The corresponding velocity distributions $P(V)$.

We next address the nature of the fluctuations of the flow above the declogging force F_c. Generally we observe highly intermittent flow immediately above the declogging or depinning transition, where regions which are temporarily clogged coexist with moving or flowing regions, while at higher drives all of the disks are flowing. In Fig. 11(a) we plot the instantaneous velocity V versus time for the system in Fig. 9(a) with $r_{\rm obs} = 1.51$ in the uniform clogged phase for $F_D/F_C = 1.0034$, just above the depinning threshold, as well as for a higher drive of $F_D/F_C = 1.67$. There are pronounced fluctuations in V just above the depinning threshold, while at the higher drive the velocity variations are reduced. The fluctuations near the depinning threshold are non-Gaussian, as shown in Fig. 11(b) where we plot $P(V)$ for the samples in Fig. 11(a). For $F_D/F_C = 1.0034$, $P(V)$ has an enhanced tail at lower drives, producing a skewed distribution, while for $F_D/F_C = 1.67$, $P(V)$ has a more symmetrical Gaussian shape. We observe similar trends for the other values of $r_{\rm obs}$.

Differences in the noise fluctuations can also be detected by computing the power spectrum of the velocity time series, $S(\omega) = |\int \exp(-2\pi i\omega)V(t)dt|^2$. In Fig. 12 we plot $S(\omega)$ for the system in Fig. 11(a). To construct this plot, we average together several time series. For $F_D/F_C = 1.0034$, the fluctuations have a $1/f^\alpha$ or broad band noise character with $\alpha = -1.5$, while for $F_D/F_C = 1.67$, we find a white noise signature with $\alpha = 0$. There are peaks in $S(\omega)$ at higher ω produced by the periodic signal from the disks encountering the obstacle lattice. The lower frequency $1/f^\alpha$ noise is associated with long time large scale changes in the disk configurations. Even under very strong fluctuations, the velocity above the depinning transition never drops to zero because this would cause the system to be permanently captured in a clogged state. In contrast, other systems with constant flux or some periodic perturbation would show intermittent flow that would be expected to have $1/f^\alpha$ noise characteristics. Studies of clogging in bottlenecks have also found intermittent dynamics including power law distributions of bursts[63,64]. The exponent $\alpha = 1.5$ is close to the value found in many other systems of driven particles moving over quenched disorder in two dimensions that exhibit strong fluctuations near depinning[41,65,66]. Another commonly observed feature is the reduction of the noise at higher drives well above the depinning threshold, as shown in Fig. 12.

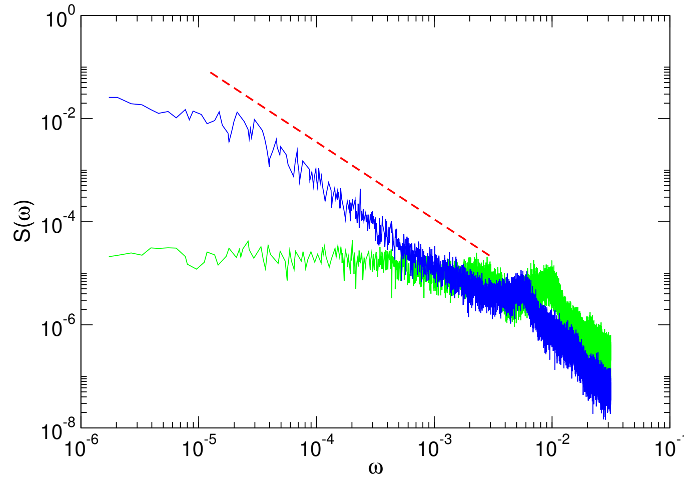

Fig. 12 The power spectra $S(\omega)$ vs ω for the system in Fig. 11(a) with $\phi = 0.68$, $\theta = 33.8^\circ$, and $r_{\rm obs} = 1.51$ at $F_D/F_C = 1.0034$ (red) and $F_D/F_C = 1.67$ (blue). The dashed line is a power law fit of the $F_D/F_C = 1.0034$ curve to $\alpha = -1.5$, while the $F_D/F_C = 1.67$ curve exhibits white noise at lower frequencies with $\alpha = 0$.

Clogging in Diluted Arrays

In the absence of obstacles, the disks would flow for any finite drive. Thus we study random dilution of the obstacle array in order to observe the transition from a clogged state to a flowing phase. We select a fraction P_d of obstacles to remove at random from the system in Fig. 9 with an undiluted value of $\phi = 0.68$, $\theta = 33.8^\circ$, and $F_D = 0.0029$, well below the depinning threshold of the undiluted sample. In Fig. 13 we plot M versus the dilution fraction P_d for $r_{\rm obs} = 1.525$, $r_{\rm obs} = 1.485$, and $r_{\rm obs} = 1.475$. For each point we average over 10 realizations, and the strongest sample-to-sample fluctuations occur near a dilution of $P_d = 0.5$. The $r_{\rm obs} = 1.475$ has no depinning threshold even when $P_d = 0$,

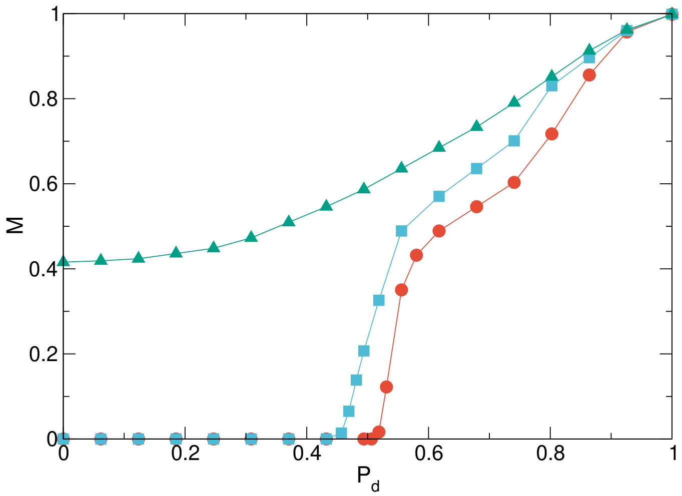

Fig. 13 The mobility M vs the dilution fraction P_d for random dilution of the square array in the system from Fig. 9 with an undiluted value of $\phi = 0.68$, $\theta = 33.8°$ and $F_D = 0.003$ at $r_{obs} = 1.525$ (red circles), 1.485 (blue squares), and 1.475 (green triangles).

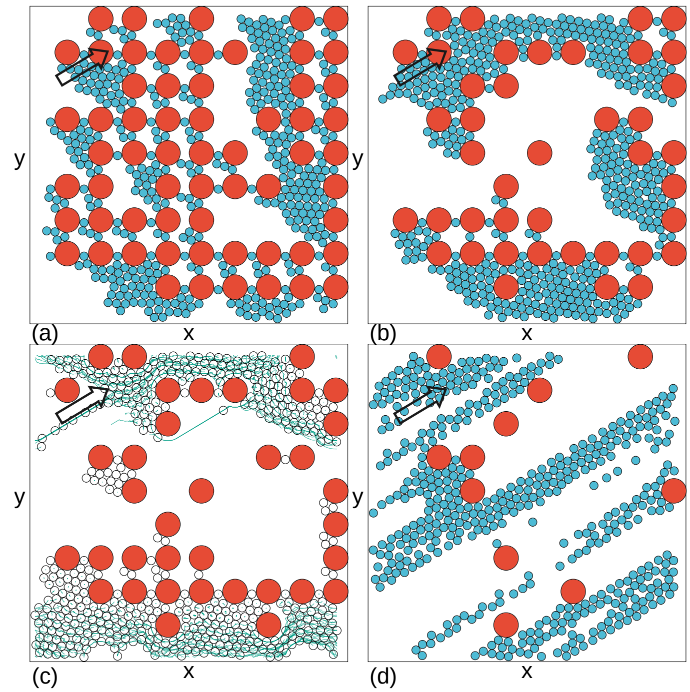

Fig. 14 The obstacle locations (red circles) and mobile disks (blue circles) for the system in Fig. 13 with an undiluted value of $\phi = 0.68$, $F_D = 0.0025$ and $\theta = 31°$ at $r_{obs} = 1.525$ under different pinning dilutions P_d. (a) The clogged phase at $P_d = 0.25$. (b) The clogged phase at $P_d = 0.494$. (c) The moving phase at $P_d = 0.56$ where green lines indicate the trajectories of the mobile disks. (d) The heterogeneous moving phase at $P_d = 0.86$.

and as P_d increases, there is a gradual increase in M which reaches a saturation value of $M = 1.0$ near $F_d = 1.0$. In the $r_{obs} = 1.525$ sample, the depinning threshold for $P_d = 0$ is $F_C = 0.07$. As P_d increases, the system remains clogged up to $P_d = 0.52$, and then there is a gradual increase in M as the dilution fraction becomes larger. In general, we find that when the $P_d = 0$ depinning threshold is finite, the dilution needs to be greater than $P_d = 0.44$ in order to unclog the system, as shown for the $r_{obs} = 1.485$ sample. This indicates that the transition from a clogged to a flowing state is probably related to a percolation transition.

As the dilution is increased, the time required for the system to organize to a steady state increases but shows pronounced fluctuations if different initializations of the mobile disk locations are used. When $r_{obs} = 1.525$, the $P_d = 0$ sample forms a uniform clogged state; however, as the dilution increases up to $P_d = 0.5$, the clogged state becomes increasingly heterogeneous. This is illustrated in Fig. 14. At $P_d = 0.25$ in Fig. 14(a), the system is spatially heterogeneous but is still clogged. The clogged state that appears at $P_d = 0.494$ just before the transition to a moving phase is shown in Fig. 14(b). For $0.52 < P_d < 0.62$, clogged regions coexist with moving regions, resulting in plastic flow as indicated in Fig. 14(c) at $P_d = 0.56$. At high dilution, the system forms a moving phase that is distinguished from the moving states found in undiluted arrays by its pronounced spatial heterogeneity, as shown in Fig. 14(d) for a sample with $P_d = 0.86$. We observe similar dynamics in the diluted systems whenever the depinning threshold is finite. In Fig. 15(a) we plot a barely clogged configuration at $r_{obs} = 1.485$ and a dilution of $P_d = 0.37$, showing a heterogeneous spanning clogged state, while in Fig. 15(b) we illustrate the moving state at $r_{obs} = 1.475$ and $P_d = 0.49$, where a few regions are locally clogged but the system remains in a flowing state. At low dilution, the clogged clusters are separated, but as the dilution increases, the clusters become larger until they nearly span the system for dilutions of $P_d = 0.5$. The time required for the system to reach a clogged state also increases with increasing dilution.

The initial conditions in the diluted system are random and are close to what would be expected in a thermalized system. The results should depend strongly the initial conditions. For example, if the disks were initialized by driving them into the sample, the system could already be in a clogged or heterogeneous state by the end of the initialization process. Additionally, when disks are removed to create the dilution, it is possible for rare configurations to appear that could cause the system to clog very rapidly or never to clog at all. This is particularly true near the dilution of $P_d = 0.5$, where the system is close to the transition between always clogging and always flowing. It would be interesting to temporarily reverse the direction of driving and then restore the drive to its original direction in order to test whether the system has some memory or whether ac driving permits it to reach a much more strongly clogged state. Such memory effects or cyclic driving will be the subject of another work.

Experimentally, our system could be realized in a setup similar to the geometry used by Stoop *et al.* with a periodic obstacle array. Samples with different obstacle sizes could be tested while the substrate is rotated with respect to the drive. Although there are many different facets that we have explored in this work, some key features that could be the focus of an experimental study include the memory effect, the critical obstacle size for clogging to occur, and the directional dependence.

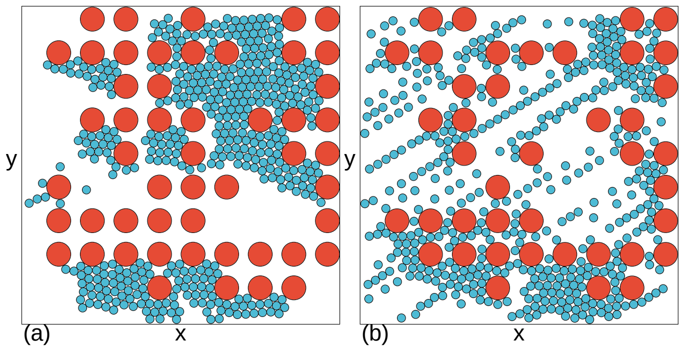

Fig. 15 The obstacle locations (red circles) and mobile disks (blue circles) for the system in Fig. 13 with an undiluted value of $\phi = 0.68$, $F_D = 0.0025$, and $\theta = 31^\circ$. (a) At $r_{\rm obs} = 1.485$ and $P_d = 0.37$ in a barely clogged state, the disk arrangement is heterogeneous. (b) A flowing state at $r_{\rm obs} = 1.475$ and $P_d = 0.494$.

Conclusions

We have examined the clogging dynamics for a monodisperse assembly of disks moving through a periodic obstacle array. We find that the susceptibility for the system to clog under fixed disk density and obstacle radius depends on the direction of drive relative to the symmetry of the obstacle lattice. The system clogs at incommensurate driving angles or for angles in the range $30^\circ < \theta < 70^\circ$; however, the range of parameters over which clogging occurs increases with increasing system density and obstacle size. The systems is least susceptible to clogging for drives centered around $\theta = 0^\circ$ and $\theta = 90^\circ$. Under a changing drive angle the system exhibits a memory effect in which the formation of a clogged state for one driving direction results in a reduced flow rate when the drive is rotated into the perpendicular direction. The memory effect is lost as the disk density or obstacle radius decreases. We observe two distinct types of clogging states: heterogeneous or phase separated clogging in which groups of disks must gradually arrange themselves into a clogged configuration, and a uniform clogged state in which the spacing between adjacent obstacles is small enough that individual disks can be trapped immediately. Since we represent the disk-disk interactions with a stiff harmonic potential, a clogged state can be unclogged by increasing the driving force and inducing a depinning transition. The disk configurations are generally uniform in the unpinned phase. For drives just above the unclogging transition, the velocity exhibits non-Gaussian fluctuations with a $1/f^\alpha$ noise characteristic, where $\alpha \approx 1.5$. At higher drives, the velocity distribution becomes Gaussian and the fluctuations have a white noise signature. We also show that a clogged to unclogged transition can be produced when the obstacle lattice is diluted through the random removal of a fraction of obstacles. The disk arrangement becomes increasingly heterogeneous for increasing dilution, and a transition to an unclogged state occurs for dilution fractions close to 0.5, indicating that the transition has a percolation character. Our results should be relevant for clogging dynamics in soft colloidal systems, emulsions, and bubbles. Similar clogging effects could also occur for magnetic bubbles, skyrmions, or superconducting vortices moving though periodic pinning or obstacle arrays.

Conflicts of interest

There are no conflicts to declare.

Acknowledgements

This work was supported by the US Department of Energy through the Los Alamos National Laboratory. Los Alamos National Laboratory is operated by Triad National Security, LLC, for the National Nuclear Security Administration of the U. S. Department of Energy (Contract No. 892333218NCA000001).

Notes and references

1 A. J. Liu and S. R. Nagel, *Nature (London)*, 1998, **396**, 21–22.
2 C. S. O'Hern, L. E. Silbert, A. J. Liu and S. R. Nagel, *Phys. Rev. E*, 2003, **68**, 011306.
3 J. A. Drocco, M. B. Hastings, C. J. O. Reichhardt and C. Reichhardt, *Phys. Rev. Lett.*, 2005, **95**, 088001.
4 A. J. Liu and S. R. Nagel, *Annual Review of Condensed Matter Physics*, 2010, **1**, 347–369.
5 C. Reichhardt and C. J. O. Reichhardt, *Soft Matter*, 2014, **10**, 2932–2944.
6 P. Olsson and S. Teitel, *Phys. Rev. Lett.*, 2007, **99**, 178001.
7 L.-N. Zou, X. Cheng, M. L. Rivers, H. M. Jaeger and S. R. Nagel, *Science*, 2009, **326**, 408–410.
8 L. M. Lopatina, C. J. Olson Reichhardt and C. Reichhardt, *Phys. Rev. E*, 2011, **84**, 011303.
9 R. S. Hoy, *Phys. Rev. Lett.*, 2017, **118**, 068002.
10 R. Candelier and O. Dauchot, *Phys. Rev. E*, 2010, **81**, 011304.
11 D. Bi, J. Zhang, B. Chakraborty and R. P. Behringer, *Nature (London)*, 2011, **480**, 355–358.
12 K. To, P.-Y. Lai and H. K. Pak, *Phys. Rev. Lett.*, 2001, **86**, 71–74.
13 C. C. Thomas and D. J. Durian, *Phys. Rev. E*, 2013, **87**, 052201.
14 D. Chen, K. W. Desmond and E. R. Weeks, *Soft Matter*, 2012, **8**, 10486–10492.
15 I. Zuriguel, D. R. Parisi, R. C. Hidalgo, C. Lozano, A. Janda, P. A. Gago, J. P. Peralta, L. M. Ferrer, L. A. Pugnaloni, E. Clément, D. Maza, I. Pagonabarraga and A. Garcimartín, *Sci. Rep.*, 2015, **4**, 7324.
16 D. Gella, I. Zuriguel and D. Maza, *Phys. Rev. Lett.*, 2018, **121**, 138001.
17 C. J. O. Reichhardt and C. Reichhardt, *J. Phys.: Condens. Matt.*, 2018, **30**, 244005.
18 S. Redner and S. Datta, *Phys. Rev. Lett.*, 2000, **84**, 6018–6021.
19 F. Chevoir, F. Gaulard and N. Roussel, *EPL*, 2007, **79**, 14001.
20 N. Roussel, T. L. H. Nguyen and P. Coussot, *Phys. Rev. Lett.*, 2007, **98**, 114502.
21 H. M. Wyss, D. L. Blair, J. F. Morris, H. A. Stone and D. A. Weitz, *Phys. Rev. E*, 2006, **74**, 061402.
22 C. Barre and J. Talbot, *J. Stat. Mech.*, 2017, **2017**, 043406.
23 C. J. Olson Reichhardt, E. Groopman, Z. Nussinov and C. Reichhardt, *Phys. Rev. E*, 2012, **86**, 061301.
24 C. Reichhardt and C. J. O. Reichhardt, *Phys. Rev. E*, 2018, **97**, 052613.

25 M. Le Blay, M. Adda-Bedia and D. Bartolo, *Proc. Natl. Acad. Sci. (USA)*, 2020, **117**, 13914–13920.

26 M. Alava, M. Dubé and M. Rost, *Adv. Phys.*, 2004, **53**, 83–175.

27 D. L. Liu, P. R. Johnson and M. Elimelech, *Environ. Sci. Technol.*, 1995, **29**, 2963–2973.

28 F. Wirner, C. Scholz and C. Bechinger, *Phys. Rev. E*, 2014, **90**, 013025.

29 E. Dressaire and A. Sauret, *Soft Matter*, 2017, **13**, 37–48.

30 Q. Liu, B. Zhao and J. C. Santamarina, *J. Geophys. Res.: Solid Earth*, 2019, **124**, 9495–9504.

31 G. Gerber, S. Rodts, P. Aimedieu, P. Faure and P. Coussot, *Phys. Rev. Lett.*, 2018, **120**, 148001.

32 G. Gerber, M. Bensouda, D. A. Weitz and P. Coussot, *Phys. Rev. Lett.*, 2019, **123**, 158005.

33 C. Brito, G. Parisi and F. Zamponi, *Soft Matter*, 2013, **9**, 8540–8546.

34 A. L. Graves, S. Nashed, E. Padgett, C. P. Goodrich, A. J. Liu and J. P. Sethna, *Phys. Rev. Lett.*, 2016, **116**, 235501.

35 P. Wentworth-Nice, S. A. Ridout, B. Jenike, A. Liloia and A. L. Graves, *Soft Matter*, 2020, **16**, 5305–5313.

36 H. T. Nguyen, C. Reichhardt and C. J. O. Reichhardt, *Phys. Rev. E*, 2017, **95**, 030902.

37 H. P ’eter, A. Libál, C. Reichhardt and C. J. O. Reichhardt, *Sci. Rep.*, 2018, **8**, 10252.

38 R. L. Stoop and P. Tierno, *Commun. Phys.*, 2018, **1**, 68.

39 S. G. Leyva, R. L. Stoop, P. Tierno and I. Pagonabarraga, *Soft Matter*, 2020, **16**, 6985–6992.

40 M. E. Cates, J. P. Wittmer, J.-P. Bouchaud and P. Claudin, *Phys. Rev. Lett.*, 1998, **81**, 1841–1844.

41 C. Reichhardt and C. J. O. Reichhardt, *Rep. Prog. Phys.*, 2017, **80**, 026501.

42 L. R. Huang, E. C. Cox, R. H. Austin and J. C. Sturm, *Science*, 2004, **304**, 987–990.

43 Z. Li and G. Drazer, *Phys. Rev. Lett.*, 2007, **98**, 050602.

44 B. R. Long, M. Heller, J. P. Beech, H. Linke, H. Bruus and J. O. Tegenfeldt, *Phys. Rev. E*, 2008, **78**, 046304.

45 J. McGrath, M. Jimenez and H. Bridle, *Lab Chip*, 2014, **14**, 4139–4158.

46 B. H. Wunsch, J. T. Smith, S. M. Gifford, C. Wang, M. Brink, R. L. Bruce, R. H. Austin, G. Stolovitzky and Y. Astier, *Nature Nanotechnol.*, 2016, **11**, 936–940.

47 R. L. Stoop, A. V. Straube, T. H. Johansen and P. Tierno, *Phys. Rev. Lett.*, 2020, **124**, 058002.

48 P. T. Korda, M. B. Taylor and D. G. Grier, *Phys. Rev. Lett.*, 2002, **89**, 128301.

49 M. P. MacDonald, G. C. Spalding and K. Dholakia, *Nature (London)*, 2003, **426**, 421–424.

50 T. Bohlein, J. Mikhael and C. Bechinger, *Nature Mater.*, 2012, **11**, 126–130.

51 M. P. N. Juniper, A. V. Straube, D. G. A. L. Aarts and R. P. A. Dullens, *Phys. Rev. E*, 2016, **93**, 012608.

52 X. Cao, E. Panizon, A. Vanossi, N. Manini and C. Bechinger, *Nature Phys.*, 2019, **15**, 776.

53 C. Reichhardt and C. J. O. Reichhardt, *Phys. Rev. E*, 2020, **102**, 022608.

54 L. Corte, P. M. Chaikin, J. P. Gollub and D. J. Pine, *Nature Phys.*, 2008, **4**, 420–424.

55 L. Milz and M. Schmiedeberg, *Phys. Rev. E*, 2013, **88**, 062308.

56 I. Regev, T. Lookman and C. Reichhardt, *Phys. Rev. E*, 2013, **88**, 062401.

57 S. Okuma, Y. Tsugawa and A. Motohashi, *Phys. Rev. B*, 2011, **83**, 012503.

58 H. Hinrichsen, *Adv. Phys.*, 2000, **49**, 815–958.

59 C. Reichhardt and C. J. O. Reichhardt, *Phys. Rev. Lett.*, 2018, **121**, 068001.

60 B. Ai, F. Meng, Y. He and X. Zhang, *Soft Matter*, 2019, **15**, 3443–3450.

61 C. Reichhardt, C. J. O. Reichhardt, I. Martin and A. R. Bishop, *Phys. Rev. Lett.*, 2003, **90**, 026401.

62 C. Reichhardt, C. J. Olson, I. Martin and A. R. Bishop, *Europhys. Lett.*, 2003, **61**, 221–227.

63 D. Gella, I. Zuriguel and J. Ortín, *Phys. Rev. Lett.*, 2019, **123**, 218004.

64 M. Souzy, I. Zuriguel and A. Marin, *Phys. Rev. E*, 2020, **101**, 060901.

65 C. J. Olson, C. Reichhardt and F. Nori, *Phys. Rev. Lett.*, 1998, **81**, 3757–3760.

66 A. Travesset, R. A. White and K. A. Dahmen, *Phys. Rev. B*, 2002, **66**, 024430.

Disks flowing through a square obstacle array clog for incommensurate driving angles, forming either uniform or heterogeneous clogged states.